Rate Constants of Mass Transfer Kinetics in Reversed Phase Liquid Chromatography

Lan Hong, Fabrice Gritti, and Georges Guiochon
Dept. of Chemistry, The University of Tennessee, Knoxville, TN, 37996 and Division of Chemical Sciences, Oak Ridge National Laboratory, Oak Ridge, TN, 37831

Krzysztof Kaczmarski
Faculty of Chemistry, Rzeszów University of Technology, 35-959, Rzeszów, Poland

DOI 10.1002/aic.10565
Published online September 2, 2005 in Wiley InterScience (www.interscience.wiley.com).

The parameters of the kinetics of mass transfer of several n*-alkylbenzenes were measured by the method of moments on a series of columns prepared with different samples of the same RPLC packing material having widely different average particle diameters, from 3 to 50 μm. These data were analyzed using the available models, and correlations. The best agreement between experimental and theoretical data was obtained under the assumption that the rate constant for the external mass transfer increases with increasing average particle size, an unexpected conclusion. It was also shown that the interpretation of the relative importance of the roles of pore diffusivity and surface diffusivity in the internal mass transfer kinetics is somewhat ambiguous and that the conclusion to be drawn from experimental results depends on the assumptions made regarding the tortuosity model and the relationship between* k_{ext} *and the average particle size.* © 2005 American Institute of Chemical Engineers *AIChE J,* 51: 3122–3133, 2005
Keywords: liquid chromatography, mass transfer kinetics, method of moments, pore diffusion, surface diffusion

Introduction

Liquid chromatography has become an important process for the extraction and/or the purification of drug intermediates in the pharmaceutical industry. It is of special interest for fragile molecules, for those that are obtained as components of very complex mixtures of similar compounds, and for difficult separations. Typical examples are the preparation of peptides, proteins, and enantiomers. In all these instances, the interest for the modeling of specific HPLC separations has much increased during the last few years because computer-assisted modeling of processes permits a considerable reduction in the time and manpower needed to start a process or to start up a unit after maintenance and brings significant economies in the design and operation costs. Process modeling is further encouraged by the strategic initiative of the Food and Drug Administration that will impact on the "current Good Manufacturing Practices" (cGMP) and will much affect chemical engineering applications in the pharmaceutical industry by requiring a better understanding of the processes involved.[1]

The modeling of the separation processes encountered in the various implementations of preparative chromatography, including simulated moving bed processes, requires an accurate knowledge of the specific equilibrium thermodynamics and equilibration kinetics involved.[2] The nature of the data required, the procedures to follow to acquire them, and the measurements to perform in order to obtain an accurate, reliable model of the competitive equilibrium isotherms of the feed components of importance are well known.[2,3] Different procedures allow the acquisition of data of increasing accuracy at an

Correspondence concerning this article should be addressed to G. A. Guiochon at guiochon@utk.edu.

increasing cost in time spent and chemicals consumed.[4] Current research aims at reducing these costs but will not change the need for these data. If the relationship between equilibrium isotherms, the calculation of elution band profiles, and the modeling of process performance is clearly established, the influence of the mass transfer kinetics on band profiles and process performance remains insufficiently understood.

For its better understanding, the kinetics of equilibration between the fluid and the solid phases in chromatography is divided into several steps that can be grouped into two broad classes, axial dispersion and the mass-transfer resistances. The former class involves axial diffusion, the consequence through Fick laws of the concentration gradient that migrates along the column, and eddy diffusion, which arises from the flow pattern. The chromatographic columns are operated under a rather slow stream of the fluid phase. In liquid chromatography, the Reynolds numbers of these flows are typically between 0.01 and 0.001, ensuring creeping flow conditions.[5] There are no significant eddies but the distribution of the average residence times along the different stream-lines has a significant width, causing eddy diffusion.[2,5] The contributions of axial dispersion to band broadening tend to decrease with increasing flow velocity.

By contrast, the effects of the mass-transfer coefficients increase with increasing mobile phase velocity. They include mass transfer between the fluid phase stream percolating through the bed and the fluid stagnant inside the particles (or in the porons, in the case of monolithic columns), diffusion through this stagnant fluid across the particles, and the kinetics of adsorption–desorption onto the solid surface. The first two of these contributions are called the external and the internal mass transfer resistances, respectively. The latter contribution has been abundantly studied and our recent results have demonstrated the importance of surface diffusion in reversed-phase liquid chromatography.[6] The external mass transfer resistance has been much less investigated. It is usually estimated in kinetic studies from the Wilson and Geankoplis correlation.[7] This remarkable equation was derived, however, from measurements carried out on a column packed with 1/4″ solid beads of benzoic acid percolated with a stream of water. The validity of this equation for columns packed with silica particles that are a thousand times smaller and exchange solutes with the external fluid through a multitude of tiny pores has never been demonstrated.

The goal of this work was to investigate the external mass transfer kinetics by determining, under linear conditions, its rate constant for a series of compounds on columns packed with the same packing material, but using lots having average particle sizes spanning a wide range, between 3 and 50 μm, hence, under experimental conditions spanning a 100-fold range of the Fick number. The dependence of the external rate constant on the particle size should provide new clues on the mass transfer-kinetics in chromatography.

Theory

General rate model (GR)

Any serious investigation of the influence of the mass-transfer kinetics on the band profiles in chromatography must use the general rate model of chromatography. Although there are no algebraic, only numerical solutions for this model, a solution is available for the Laplace transform in the linear case. This solution cannot be inverted into the time domain. However, its moments can be derived using simple algebraic manipulations. This approach constitutes the one that was followed in this work.

The following modified general rate (GR) model was used.[8] It consists of two equations.

A mass transport equation for the mobile phase percolating through the bed

$$\varepsilon_e \frac{\partial C}{\partial t} + u \frac{\partial C}{\partial x} = \varepsilon_e D_L \frac{\partial^2 C}{\partial x^2} - \sum_i \left(\frac{(1 - \varepsilon_{e,i}) \cdot 3 \cdot k_{ext}(C - C_{p,i}\,(r = R_i))}{R_i} \right) \quad (1)$$

A mass transport equation for the liquid stagnant in the pores of the solid phase

$$\varepsilon_p \frac{\partial C_{p,i}}{\partial t} + (1 - \varepsilon_p) \frac{\partial q_i}{\partial t} = D_{eff} \frac{1}{r^2} \frac{\partial}{\partial r} \left(r^2 \frac{\partial C_{p,i}}{\partial r} \right) \quad (2)$$

In these equations, C and C_p are the concentrations of the solute in the bulk liquid stream outside the particle and in the stagnant liquid phase in the pores, respectively, q is the concentration of the adsorbed component, t is the time, r is the distance from the particle center, R is the particle radius, ε_e is the external porosity, ε_p is the internal or particle porosity, and D_{eff} is the effective diffusivity coefficient. Subscript i denotes the i-th fraction of the particle-diameter distribution (see later), and the external porosity ε_{ei} is a hypothetical external porosity when only the i-th fraction exists, calculated by use of the relationship

$$\varepsilon_{e,i} = 1 - (1 - \varepsilon_e) \frac{V_i}{V_a} \quad (3)$$

where V_i is the volume of the i-th fraction and V_a is the total volume of adsorbent.

The GR model (Eqs. 1 and 2) was coupled with typical boundary and initial conditions, assuming Danckwerts boundary conditions for Eq. 1, continuity of the mass transfer on the outer surface of the particle, and a symmetrical concentration distribution inside the particles. It was also assumed that the initial concentration of each experiment (elution) was equal to zero.

Theory of second moment analysis

The chromatographic band profiles were analyzed using the conventional method of moments.[2,6,9–13] Information on thermodynamics of equilibrium between the mobile and the stationary phase and on the mass-transfer kinetics between the two phases of the system is obtained from the first absolute moment and the second central moment, respectively. The first absolute moment (μ_1), and the second central moment (μ_2') of the chromatographic peaks are expressed as follows

$$\mu_1 = \frac{\int C(t)t\,dt}{\int C(t)\,dt} = \frac{L}{u_0} \delta_0 \quad (4)$$

$$\mu_2' = \frac{\int C(t)(t-\mu_1)^2 dt}{\int C(t)dt} \tag{5}$$

where $C(t)$ is the chromatographic band profile, L is the length of the column, and u_0 the superficial mobile phase velocity. The second central moment is related to the different kinetic characteristics of the column, as follows

$$\mu_2' = \frac{2L}{u_0}(\delta_L + \delta_f + \delta_d) + (\mu_2')_{inj} + (\mu_2')_{sys} \tag{6}$$

$$\delta_L = \frac{\varepsilon_e D_L \delta_0^2}{u_0^2} \tag{7}$$

$$\delta_f = (1-\varepsilon_e)(R/2k_{ext})(\varepsilon_p + (1-\varepsilon_p)K)^2 \tag{8}$$

$$\delta_d = (1-\varepsilon_e)(R^2/15D_{eff})(\varepsilon_P + (1-\varepsilon_p)K)^2 \tag{9}$$

$$\delta_0 = \varepsilon_e + (1-\varepsilon_e)(\varepsilon_P + (1-\varepsilon_P)K) \tag{10}$$

where $(\mu_2')_{inj}$ and $(\mu_2')_{sys}$ denote the contributions to the second central moment arising from the injection of the probe compound into the stream of mobile phase and from dispersion in the extra-column void volumes of the instrument, respectively. δ_L, δ_d, and δ_f are the contributions to μ_2' of axial dispersion, the fluid-to-particle mass-transfer resistance, and intraparticle diffusion, respectively. The other parameters in these equations are: ε_e, the external (bed) porosity ε_p, the internal (particle) porosity, R, the particle radius, k_{ext}, the external mass transfer coefficient, D_{eff}, the coefficient of effective diffusivity, and $K = q/C$, the equilibrium constant. The concentrations in the fluid phase, C, and at the adsorbent surface, q, are referenced to the fluid volume and to the adsorbent matrix volume, respectively.

Equation 6 shows that the contributions to the second moment of the band of each source of mass transfer resistance are separate and additive. The first and the second moments are simply related to the number of theoretical plates N, of the column, and to its high equivalent to a theoretical plates (HETP), H, namely

$$N = \frac{\mu_1^2}{\mu_2'} \tag{11}$$

$$H = \frac{L}{N} = \frac{L\mu_2'}{\mu_1^2} \tag{12}$$

By applying Eqs. 4 to 6 to Eq. 12, the HETP is expressed as follows

$$H = \frac{2u_0\varepsilon_e}{\delta_0^2}(\delta_L + \delta_f + \delta_d) \tag{13}$$

By applying Eq. 7 to 9 to Eq. 13 we obtain the form

$$H = H_L + H_k + H_D = \frac{2\varepsilon_e D_L}{u_0} + \frac{2u_0(1-\varepsilon_e)(\varepsilon_P + (1-\varepsilon_P)K)^2}{\delta_0^2}\left(\frac{R}{3k_{ext}} + \frac{R^2}{15D_{eff}}\right) \tag{14}$$

For the sake of simplification, we define the following auxiliary parameters, A and H_0

$$A = \frac{(1-\varepsilon_e)(\varepsilon_P + (1-\varepsilon_P)K)^2}{\delta_0^2} \tag{15}$$

$$H_0 = \frac{\delta_f + \delta_d}{\delta_0^2} = A\left(\frac{R}{3k_{ext}} + \frac{R^2}{15D_{eff}}\right) \tag{16}$$

Both A and H_o are independent of the mobile phase flow velocity, insofar as the dependency of k_{ext} on the mobile phase velocity can be neglected in the increment investigated. Now, Eq. 12 can be rewritten as follows

$$H' = \frac{\mu_2'}{\mu_1^2}\frac{L}{2u_0} = \frac{\varepsilon_e D_L}{u_0^2} + H_0 \tag{17}$$

The HETP used in conventional chromatography is reported in length units. However, the parameter defined in this work H' is reported in time units.

It should be noted that the equilibrium constant, which is included in the above equations, can be easily derived from the experimental parameters and is given by

$$K = \frac{(\delta_o - \varepsilon_e)}{(1-\varepsilon_e)(1-\varepsilon_p)} - \frac{\varepsilon_p}{(1-\varepsilon_p)} \tag{18}$$

Theoretical calculation of the molecular diffusivity, the dispersion coefficient and the external mass transfer coefficient

In this work all the mass transfer kinetic parameters and the dispersion coefficient parameter were determined experimentally. The obtained results were compared with theoretical calculation of these parameters based on probably most frequently used correlations.

The External Mass-Transfer Coefficient. The external mass-transfer coefficient was calculated from the generally accepted correlation, the Wilson-Geankoplis equation[7] valid according to these authors for $0.0015 < \mathrm{Re} < 55$. This includes the range under which liquid chromatography is carried out.

$$Sh = (1.09/\varepsilon_e)Sc^{1/3}\mathrm{Re}^{1/3} \tag{19}$$

This equation relates the Sherwood number Sh, a function of the external mass transfer coefficient, to the Schmidt (Sc) and the Reynolds (Re) numbers. These numbers are defined by

$$\mathrm{Re} = \rho u d/\eta \tag{20}$$

$$Sc = \eta/\rho D_m \tag{21}$$

$$Sh = k_{ext}d/D_m \tag{22}$$

From the correlation Eq. 19, it follows that the external mass transfer rate constant is inversely proportional to the particle diameter to the power (2/3).

$$k_{ext} = \frac{1.09(u_0)^{1/3}}{\varepsilon_e}\left(\frac{D_m}{d}\right)^{2/3} \tag{23}$$

In the earlier equation, η is the mobile phase viscosity and ρ its density. This relationship permits the calculation of k_{ext} knowing the molecular diffusivity, D_m, of the solute in the mobile phase. Because the exact value of D_m is seldom available, however, it must be estimated. There are several different approaches available. The one most frequently used in the HPLC literature is the Wilke-Chang Eqs. 2, 12, 14, which is claimed to be accurate within 10% for small to medium-size molecules. Its formulation is

$$D_m = 7.4 \times 10^{-8} T \frac{(\alpha_A M_s)^{0.5}}{\eta V_A^{0.6}} \tag{24}$$

where T is the absolute temperature, V_A is the molar volume of the solute at its normal boiling point (calculated from LeBas correlation), M_s is the molecular weight of the fluid phase, η is the fluid viscosity (in cP), and α_A is the association factor for the fluid which accounts for the solute-solvent interactions. This factor is 1.9 for methanol and 2.6 for water.

Dispersion Coefficient. The dispersion coefficient was calculated from the Gunn[15] equation

$$\frac{\varepsilon_e D_L}{du_0} = B(1 + \sigma_v^2)^2 + \frac{\sigma_v^2}{2} + \frac{\varepsilon_e}{\tau\,\mathrm{Re}\,Sc} \tag{25}$$

with

$$B = \left\{\frac{\mathrm{Re}\,Sc}{4\alpha_1^2(1-\varepsilon_e)}(1-p)^2 + \frac{(\mathrm{Re}\,Sc)^2}{16\alpha_1^4(1-\varepsilon_e)^2} \times p(1-p)^3\left[\exp\left(\frac{-4\alpha_1^2(1-\varepsilon_e)}{p(1-p)\mathrm{Re}\,Sc}\right) - 1\right]\right\} \tag{26}$$

where α_1 is the first root of the zero-order Bessel function, τ is the bed package tortuosity factor (assumed to be equal to 1.4), and σ_v^2 is the dimensionless variance of the distribution of the ratio between the local fluid linear velocity and the average velocity over the column cross-section. In this work, this variance was assumed to be equal to zero. Finally, p is a parameter defined by

$$p = 0.17 + 0.33\,\exp(-24/\mathrm{Re}) \tag{27}$$

The other popular correlation between the flow velocity of the stream percolating through the bed and the axial dispersion coefficient is the following equation elaborated by Chung and Wen[16]

$$\varepsilon_e Pe = 0.2 + 0.011\,\mathrm{Re}^{0.48} \tag{28}$$

with Pe being the particle Peclet number ($Pe = ud/D_L\varepsilon_e$), and Re given by Eq. 20.

Particle-size distribution

A relationship can be derived easily between the first two moments of the elution bands, the column HETP under linear conditions, and the parameters of the general rate model if the column bed is assumed to consist in spherical particles having all the same diameters. However, all actual packing materials have a particle-size distribution (PSD) of finite width. Typical examples of the PSD of contemporary packing materials and adsorbent particles are discussed by Neue.[17] For practical calculations, the PSD is replaced by the mean-particle diameter. There exist several methods to calculate the mean diameter of a particulate material, but for the description of the mass transfer processes, such as those that take place in chromatography, the volume moment mean diameter, noted d_{43}, is recommended[17]

$$d_{43} = \frac{\sum_i n_i d_i^4}{\sum_i n_i d_i^3} \tag{29}$$

In this equation, n denotes the number of particles of size d, and the subscript i denotes the i-th fraction of the distribution. Recently it was proved[8] that the band profiles calculated from the PSD and those derived from the volume moment mean, d_{43}, for different isotherm models and for the particle dia. of 5 [μm], the most frequently used in HPLC, are practically identical.

Since in this work packing materials with average particle diameters between 3 and 50 [μm] were used, we decided to check whether the influence of the PSD on the first and second moments was significant (see later).

Experimental

Equipment

An HP 1090 (Hewlett-Packard, Palo Alto, CA) liquid chromatograph was employed for all the experimental determinations. The instrument is equipped with a multisolvent delivery system, an automatic sample injector with a 100-L loop, a diode array UV-detector and a computer data station that controls its operation. The signal of the UV detector was acquired at a wavelength of 254 nm.

Mobile phase and chemicals

The mobile phase used was a mixture solution of methanol and water (70:30 v/v). Methanol and water were HPLC grade solvents from Fisher Scientific (Fair Lawn, NJ). Thiourea was purchased from Sigma Chemicals (St. Louis, MO). The solutes studied, toluene, ethylbenzene, propylbenzene, butylbenzene, and amylbenzene were purchased from Aldrich Chemical (Milwaukee, WI).

Table 1. Characteristics of the Columns Used

Description	3 [μm]	5 [μm]	10 [μm]	15 [μm]	50 [μm]
Mean particle size. Average from several particle size analyses [μm]	3.74	5.21	10.6	14.92	47.1
Error of mean particle size evaluation	±10%	±6%	±6%	±7.5%	—
Particle distribution, 90/10%[a]	1.57	1.49	1.59	1.54	1.82
Pore diameter, Å	103	98	101	107	—
Surface area [m^2/g]	383	398	386	388	—
Total carbon, %	17.35	18.13	17.07	15.56	—
Surface coverage [μmol/m^2]	3.48	3.57	3.03	2.96	—
Total porosity[b]	0.603	0.592	0.61	0.642	0.612
External porosity[b]	0.362	0.369	0.371	0.379	0.37
Internal porosity[b]	0.378	0.353	0.38	0.423	0.384

[a]Ratio of the diameters below which 90% and 10% of the particles, respectively, are found.
[b]Values measured in our laboratory.

Chromatographic conditions

Sets of identical experiments were carried out under different flow rates on a series of stainless steel columns (all 150 × 4.6 [mm]). Five columns were packed by the manufacturer with Luna C_{18} (Phenomenex, Torrance, CA) in different average particle sizes, 3, 5, 10, 15, and 50 [μm]. This packing material is made of spherical particles of porous silica, chemically bonded with octadecylsilane. Their chemical properties are broadly similar as far as alkylaromatics are concerned. The details of the column parameters, as supplied by the manufacturers, are shown in Table 1. These columns are similar to one that was investigated by Kele[18] but they belong to more recent lots and most of them have different particle sizes. The column temperature was kept constant at 25.0°C.

To achieve accurate results, the column was equilibrated for at least three hours prior to any measurement when the mobile phase composition was changed. The run-to-run reproducibility of the instrument was characterized by a RSD of the peak area which was better than 0.50% (six replicates) for an injection volume of 5 μL. The first and second moments of the elution bands of the solutes were measured for the following mobile phase flow rates: 0.8, 1.0, 1.2, 1.5, and 1.8 [mL/min] for average particle sizes of 5, 10, and 15 [μm]; 0.6, 1.0, 1.2, and 1.4 [mL/min] for an average particle sizes of 3 [μm]; and 1.2, 2.0, 2.4, and 2.8 [mL/min] for an average particle size of 50 [μm].

The total porosity ε_t, of each column was derived from the retention volume of thiourea, that was considered to be unretained on all the columns, an assumption consistent with the results previously obtained by this group under the experimental conditions used here. The external porosity ε_e, was obtained from measurements carried out under ISEC mode (see later, section 3.6). The internal porosity ε_P, was calculated according to the conventional equation $\varepsilon_t = \varepsilon_e + (1 - \varepsilon_e)\varepsilon_p$. The porosities are also listed in Table 1.

Selection of solutes and columns

Toluene, ethylbenzene, propylbenzene, butylbenzene, and amylbenzene were tested with different columns. It was found that ethylbenzene, propylbenzene, and butylbenzene, eluted on columns packed with particles having dia. of 3, 5, 10, 15, and 50 [μm], could provide peaks of suitable width for an accurate measurement of the second moment under the experimental chromatographic conditions required. The peak of toluene was too narrow and the peak of amylbenzene had too high a retention time, more than 60 min. The use of either solute would have resulted in excessively large errors in the measurement of their second moments.

Procedures for moment analysis

In this work, all the measurements reported were carried out under linear chromatographic conditions. The lowest sample size that the sampling system of the instrument could deliver (5 [μL]) was used. Dilute solutions (ca. 130–300 ppm, v/v) were used for the measurements. Nevertheless, the signal to noise ratio was sufficient to afford precise values of the peak moments. The corresponding elution peaks were recorded, and the first and second moments were obtained from the reports generated by the program of the HP ChemStation for LC-3D. The start and end points of the peaks were automatically selected by the parameter of slope sensitivity. The accuracy and precision of the moments measured by the Chemstation has been previously assessed, using the same instrument.[19]

The values of the extra-column volumes between the injection valve, and the column and between the column and the detector were derived from the retention volumes of the solute measured on the instrument with the column being replaced with a zero-volume connector. The contributions of $(\mu_2')_{inj}$ and $(\mu_2')_{sys}$ to the second moment μ_2', of the solute were calculated by measuring the second moment of the solute on the system with a zero-volume connector, and without column at each flow rate and subtracting it from the second moment of the solute.

Determination of the external porosity of the column via ISEC

The external porosity of a column is conveniently evaluated using the method of inverse size exclusion chromatography (ISEC).[20,21] As commonly understood, conventional SEC permits the separation of molecules according to their size. It uses as the stationary phase a porous material of known pore-size distribution, under experimental conditions (that is, with a mobile phase) such that the sample components do not adsorb on the pore surface of the packing material. There is a general relationship between the size of a molecule, and the size of the pores from which it is excluded. In ISEC, the converse principle is exploited. The pore-size distribution of an adsorbent is

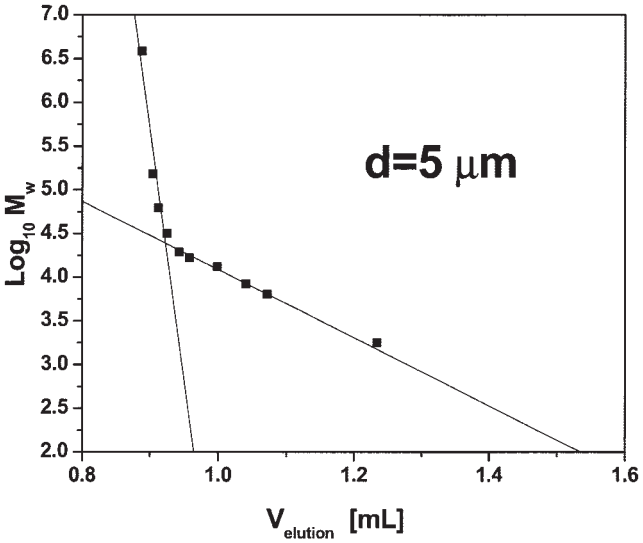

Figure 1. Logarithm of the molecular mass of the samples vs. their retention volumes for a series of polystyrene standards.

derived from the retention volumes of standard samples of known molecular mass. More simply, in the present case, the external and internal porosities are derived from the experimental relationship between the molecular mass of the polymeric compounds used and the average size of the pores from which they are excluded. Accordingly, estimate of the pore-size distribution of the packing material studied, and of its external porosity can be derived from this plot. The successful application of ISEC requires that a few simple conditions be fulfilled:[21] there should be no adsorption of the polymeric samples on the stationary phase; the standard molecules should not aggregate; all their chains should remain in the same conformation; there should be instantaneous equilibrium between the two phases of the system during the whole experiment; the stationary phase should remain rigid (that is, should not swell). Experimental investigations showed that tetrahydrofuran or methylene chloride are ideal for performing such measurements on RPLC packing materials, using polystyrene samples.

Figure 1 shows a typical result obtained, the plot of the logarithm of the molecular mass of the samples vs the retention volumes of a series of polystyrene standards (with molecular masses between 1,780 and 3,840,000). Samples of 10 μL of a 1 g/L solution were injected for each polystyrene standard. The chromatograms were recorded at 265 nm. Two linear regression lines (solid lines) identify two specific regions in the pore-size distribution corresponding to the interparticle, and the intraparticle pore volumes, respectively. The intersection of these two linear regression lines gives the value of the external pore volume, which allows the calculation of the external porosity.[20,21]

The values obtained for the external column porosities are summarized in Table 1, together with the values calculated for the internal porosities. The column-to-column fluctuations of the results reflect a combination of the precision of the measurements, and the reproducibility of the packing procedure.

Results and Discussion

Influence of the particle-size distribution on the second moments

Influence of the Mean Particle Size. The actual mean particle size can differ by as much as 10% from the nominal value, as seen in Table 1. To gain an accurate knowledge on how the value of the particle-mean diameter can influence the second moment, numerical solutions of the GR model were calculated for particle diameters equal to 5 and 5.3 [μm], on the one hand, to 50 and 53.5 [μm], on the other hand. The mobile phase velocity was assumed to be equal 1 [ml/min]. The other GR model parameters (the porosities, the dispersion coefficient, and the mass-transfer coefficients) were taken from those derived from our experimental data and which are reported later in this work or can be found in Table 1.

According to the calculated peak profiles, the relative difference between the second moment calculated for the two pairs of actual particle diameters was derived according to the equation

$$\Delta\mu = \frac{\mu'_{2,d2} - \mu'_{2,d1}}{\mu'_{2,d1}} \tag{30}$$

The indices $d1$ and $d2$ in Eq. 30 denote the smaller and the higher particle diameters, respectively. The relative difference $\Delta\mu$ for dia. of 5 and 5.3 [μm] (a relative difference of 6%) was 18%; for dia. 50 and 53.5 [μm] (a relative difference of 7%), it was about 13%.

The Particle-Size Distribution. The equations giving the peak moments (Eqs. 4 and 5) are correct only when it is assumed that all the particles in the bed have the same diameter. However, the particles of all particulate materials have a certain diameter distribution. The integral distribution of the volume fraction f, as a function of the particle diameter is presented in Figure 2 for the 15 μm particles. This result is typical of those obtained for all the materials investigated in this work. The PSD were determined with a Mastersizer (Mavern Instrument) by the column supplier.

To investigate the influence of the PSD on the second moment, numerical solutions of the GR model were calculated. Figure 3 compares the peak profiles obtained for a packing material made of uniform particles having a diameter equal to the mean moment volume diameter (d_{43} = 46.49 [μm]), and for the correct PSD. The peak obtained with the actual PSD is slightly shorter and wider than the one corresponding to identical beads. For particles having a smaller size, these discrepancies are smaller. The relative differences between the values calculated for the first moment of the peaks by the two methods just described were less than 1×10^{-6}. The relative difference between the second moments

$$\Delta\mu = \frac{\mu'_{2,PSD} - \mu'_{2}}{\mu'_{2,PSD}} \tag{31}$$

is reported in Table 2. In this equation, $\mu'_{2,\mathrm{PSD}}$ and μ'_2 denote the second moments calculated with the actual PSD, and with the mean-particle diameter, respectively.

As seen in Table 2, the relative differences between the correct value of the second moment and the one calculated with

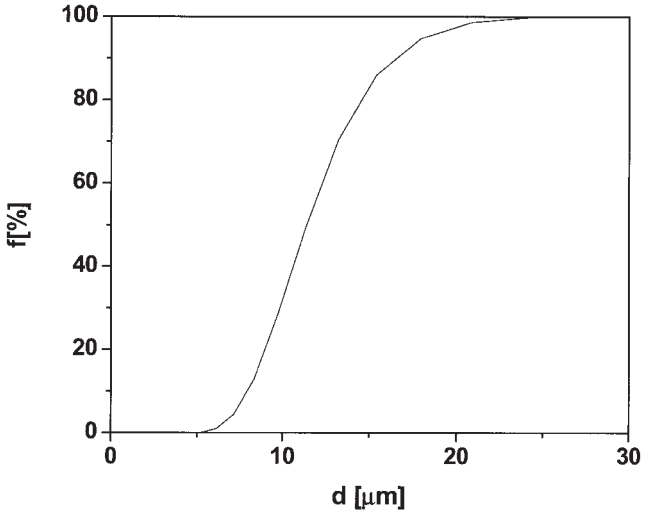

Figure 2. Integral volume fraction *f*, or ratio of the volume of the particles with a diameter less than *d* to the total volume of the particles vs. the particle diameter.

The volume mean diameter of this material is $d_{43} = 12.77$ [μm].

the average particle size is negligible for particle diameters less than about 10 [μm]. For a nominal particle diameter of 50 [μm], the relative difference can be as large as 7%. It decreases slowly with increasing mobile phase flow velocity.

Determination and calculation of the axial dispersion coefficient

According to Eq. 17, a series of elution chromatograms were run for each probe compound, on each column, at different mobile phase flow rates. The dependence of H' on the mobile phase velocity results from the effect of axial dispersion. A plot of $(\mu'_2 L)/(2\mu_1^2 u_0)$ vs. $1/u_0^2$ should be a straight line, having for

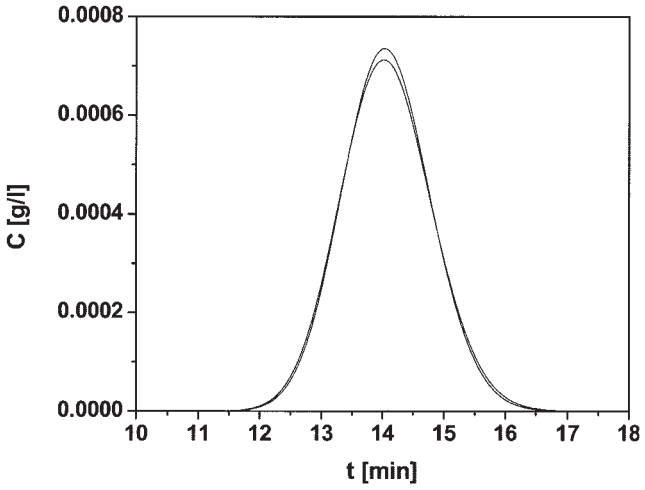

Figure 3. Comparison between the peak profiles calculated by GR for the average particle dia. d_{43} = 46.49 [μm] (higher peak), and for the true PSD (smaller peak).

Table 2. Relative Differences Between the Moments Calculated from the PSD and from the Mean Particle Diameter

d_{43} [μm]		46.49		12.7	5.16
u_o [ml/min]	0.8	1	1.4	1	1
$\Delta\mu$ [−]	0.071	0.063	0.056	0.028	0.0098

slope the coefficient of axial dispersion D_L, and for intercept, the value of H_0. The plots of H' vs. $1/u_0^2$ for the five columns studied are shown in Figure 4. The experimental data points span nearly perfect straight lines for all five-particle diameters investigated. All the R^2 values were larger than 0.99. From this result, it follows that the value of H_o is practicably independent of the fluid velocity in the range studied, which shows that, in this range, the coefficient k_{ext} is practically constant. The values of the axial dispersion coefficient calculated from the slopes of the straight lines in Figure 4 are reported in Table 3, and compared with the theoretical value derived from Gunn correlation, Eq. 25. As expected, the experimental values of the dispersion coefficient increase with increasing particle size. However, there is no systematic relationship between the axial dispersion coefficient, and the molecular diffusivity of ethylbenzene, propylbenzene and butylbenzene, which decrease in this order.

This result suggests that the influence of molecular diffusivity on the apparent dispersion coefficient is rather minor, meaning that the contribution of eddy diffusion is much larger than that of molecular axial diffusion.

The two values of D_L derived from Eq. 25, and reported in Table 3 were calculated for the smallest, and the largest mobile phase velocities for which moment measurements were carried out, for each particle diameter. Except for the largest particle diameter for which this ratio is about two, the second value (at the largest flow rate) is between three and four times larger than the first one. The agreement between the calculated and the experimental values is relatively good for small particle diameters (3 and 5 [μm]), the experimental values being intermediate between the two values derived from the calculations. For larger particle diameters (10 to 50 μm), the calculated dispersion coefficient is about two to three times larger than the experimental one. The worst agreement was obtained for the medium particle size. Finally, values of the dispersion coefficient calculated from Eq. 28 are given in the last column of Table 3. These values are generally much larger than the experimental ones, especially in the size range most frequently used in chromatography. From these results it seems that Gunn correlation approximates better our experimental data.

Relatively large discrepancies between the experimental and the theoretical values can result from our neglecting so far the influence of the PSD, and using the average particle size in the calculations of the moments and of the axial dispersion coefficients. We need to evaluate the possible effect due to PSD on the determination of an estimate of the apparent dispersion coefficient. The largest difference between the second moments derived from the mean particle diameter and from the PSD was found earlier to take place for the largest particle diameter (see Table 2). Because the finite width of the particle-size distribution causes an increase in the second moment, it will result in the experimental value of H' being larger than theoretical value that would be calculated for a bed of identical

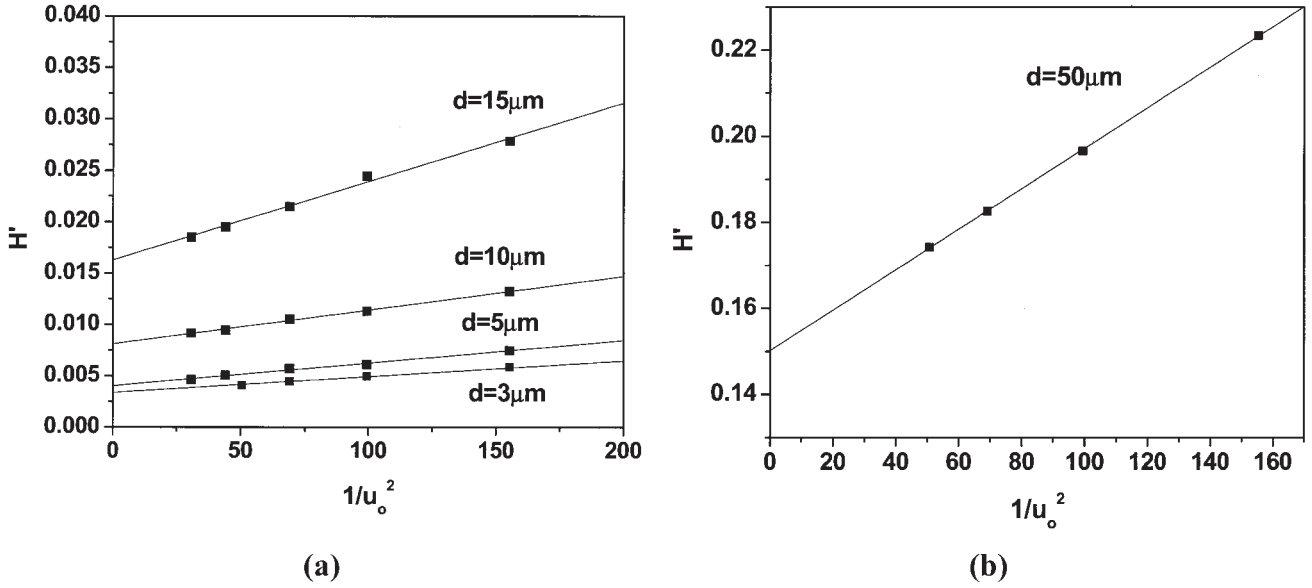

Figure 4. Typical plot of H' vs. $1/u_0^2$ according to Eq. 17.

H' is derived from the second moment of the propylbenzene peaks at different mobile phase flow velocities. (a) Particles between 3 and 15 μm, and (b) Particles of 50 μm.

particles. Moreover, the value of the second moment depends on the mobile phase velocity and decreases with increasing fluid velocity. All this means that the fact that the PSD has a finite width affects the slope of the straight lines in Figure 4.

To account for the influence of the PSD and evaluate the maximum possible error made on the dispersion coefficient, the H' values calculated for the largest particle size were multiplied by $(1 - \Delta\mu)$, with $\Delta\mu$ given in Table 2. The sign minus accounts for the fact that the second moment of a hypothetical bed of identical particles is smaller than that of a bed of particles with a PSD having a finite width. The difference between the two values of the dispersion coefficients calculated after and before this correction was less than 5%. So, the error made from neglecting the finite width of the PSD cannot explain the differences observed between the experimental values of D_L, and those derived from classical correlations, Eqs. 25, 28. Neither can the uncertainty of the actual particle size can explain these discrepancies. The difference between the values of D_L calculated from Eq. 25 for particle dia. of 10 and 9 [μm] is less than about 15%.

Determination of the external mass-transfer coefficient and the effective diffusivity

According to Eq. 17, the value of H_o can be derived from the intercept of the straight lines with the ordinate axis. This value of H_o is affected with the systematic error caused by neglecting the influence of the PSD. However, we did not try to correct for this error because of the uncertainty of the actual mean-particle diameter, as just discussed, and because the error is relatively small, anyway.

The value of H_o is directly related to the rate constant of the external mass transfer kinetics and to the effective diffusivity. Equation 16 shows that the effective diffusivity can be derived from a plot of H_o vs. R^2, as the slope of the straight line obtained while the intercept of this plot with the ordinate axis

Table 3. Calculated and Measured Values of D_L

	D_L [cm^2/s]						
	Ethylbenzene		Propylbenzene		Butylbenzene		
d [μm]	Exp[a]	Eq. 25[b]	Exp[a]	Eq. 25[b]	Exp[a]	Eq. 25[b]	Eq. (28)[b]
3.74	4.28×10^{-5}	1.45×10^{-5} 5.86×10^{-5}	4.23×10^{-5}	1.51×10^{-5} 6.06×10^{-5}	3.53×10^{-5}	1.55×10^{-5} 6.38×10^{-5}	1.1×10^{-4} $2.6\ 10^{-4}$
5.21	6.30×10^{-5}	2.16×10^{-5} 8.61×10^{-5}	5.96×10^{-5}	2.28×10^{-5} 9.23×10^{-5}	7.15×10^{-5}	2.37×10^{-5} 9.72×10^{-5}	2.1×10^{-4} $4.7\ 10^{-4}$
10.6	8.13×10^{-5}	1.32×10^{-4} 5.37×10^{-4}	8.88×10^{-5}	1.42×10^{-4} 5.67×10^{-4}	9.29×10^{-5}	1.49×10^{-4} 5.89×10^{-4}	4.3×10^{-4} $9.5\ 10^{-4}$
14.92	1.34×10^{-4}	2.48×10^{-4} 9.08×10^{-4}	2.02×10^{-4}	2.56×10^{-4} 9.50×10^{-4}	1.46×10^{-4}	2.68×10^{-4} 9.81×10^{-4}	6.0×10^{-4} $1.3\ 10^{-3}$
47.1	1.17×10^{-3}	1.52×10^{-3} 3.53×10^{-3}	1.27×10^{-3}	1.58×10^{-3} 3.61×10^{-3}	1.28×10^{-3}	1.62×10^{-3} 3.66×10^{-3}	1.9×10^{-3} 3.3×10^{-3}

[a]Values derived from the slopes of the lines in Figure 4, using Eq. 17.
[b]Values calculated from Eq. 25 or 28.

gives the external mass-transfer coefficient. However, such a simple method cannot be used in this study because the external mass-transfer coefficient is a function of the particle size. This problem is usually circumvented by calculating the external mass transfer coefficient from one of the generally accepted correlations and then using Eq. 16 to calculate the effective diffusivity.[6,13]

One of the most widely accepted correlations for the rate constant of the external mass transfer kinetics is the Wilson-Geankoplis equation.[7] It indicates that the external mass-transfer coefficient should be inversely proportional to $(d)^{2/3}$. The correlation is valid for $0.0015 < \mathrm{Re} < 55$. In our experiments, the Reynolds number was between: 0.001 and 0.04, so it was around the low end of the range of validity of the Wilson-Geankoplis equation. In this work, we will not assume any *a priori* correlation for the external mass-transfer coefficient, but will estimate directly k_{ext} from the dependency of H_o on the particle diameter, using the following equation

$$H_0 = A^R\left(\frac{R}{3k_{ext}} + \frac{R^2}{15\left(\frac{D_m\varepsilon_p^R}{\gamma} + (1-\varepsilon_p^R)*D_s*K^R\right)}\right) \quad (32)$$

This equation is derived from Eq. 16 assuming that the contributions of the pore diffusivity and the surface diffusivity D_s, to the effective diffusivity are parallel. Thus,

$$D_{eff} = \frac{D_m\varepsilon_p^R}{\gamma} + (1-\varepsilon_p^R)*D_s*K^R \quad (33)$$

the superscript R in the last two equations was added to emphasize that parameters A, ε_p, and K depend all on the particle size. This means that the parameters listed earlier, have different values for different columns filled with particles of the same adsorbent but having different diameters. The tortuosity parameter was calculated from one of the following two correlations[2,12]

$$\gamma = \frac{(2-\varepsilon_p)^2}{\varepsilon_p} \quad (34)$$

$$\gamma = \varepsilon_p + 1.5(1-\varepsilon_p) \quad (35)$$

As indicated earlier, the Wilson-Geankoplis correlation[7] states that k_{ext} is proportional to $1/(R)^{2/3}$. On the other hand, for a stagnant fluid phase, the external mass-transfer coefficient is inversely proportional to the particle dia.,[12] and $k_{ext} = D_m/R_p$.

Taking all that into account, it was assumed that

$$k_{ext} \approx \frac{\alpha}{R_p^\beta} \quad (36)$$

combination of Eqs. 32, 33, 36 and either Eq. 34 or 35 gives an equation with three unknown parameters, α, β, and D_s. However, there are only five experimental data points, for the five different particle diameters used in this work. This is too small a data set to perform a robust estimation of all three parameters. To avoid this problem, a value of β was assumed arbitrarily in Eq. 36, and the other two parameters were then estimated, using the Levenberg—Marquardt method modified by Fletcher.[22] The external mass transfer coefficient was calculated on the basis of the assumed value of β and of the estimated value of α. Typical examples of the results obtained for this estimation are reported in Tables 4 and 5.

Table 4 lists the values of the external mass-transfer coefficient k_{ext}, calculated for propylbenzene on the five columns packed with particles of five different diameters, assuming that the parameter β in Eq. 36 is equal 2/3[7] and that the tortuosity factor is given by Eq. 34. The values calculated for this coefficient, listed in the column "experiment," are compared with those calculated from Eq. 23, listed in the column "theory." The smaller and the higher values in this column were calculated from the experimental data corresponding to the minimum and maximum mobile phase velocities. The calculated values are about twice smaller than the experimental ones. For the other compounds studied, the results (not shown) are very similar.

The estimated values of the external mass-transfer coefficient, and of the surface diffusivity obtained for different values of the parameter β in Eq. 36, and for all the compounds studied are given in Table 5. In the last column of this table, the value of the Fisher test, F, is also given. The higher F, the better the estimate. The value $\beta = 2/3$ is that of the Wilson-Geankoplis correlation. The value $\beta = 1$ corresponds to a stagnant fluid. A value $\beta = -1$ corresponds to the assumption

Table 4. Comparison of Experimental and Calculated Rate Constants of External Mass Transfer for Different Average Particle Diameter

	k_{ext}[a] [cm/s]	
d [μm]	Experiment	Theory[b]
3.74	0.2	0.07–0.094
5.21	0.162	0.057–0.082
10.6	0.101	0.051–0.039
14.92	0.0806	0.031–0.041
47.1	0.0377	0.014–0.019

[a]Values for *n*-propylbenzene.
[b]Values calculated using Eq. 23. Tortuosity factor from Eq. 34. $\beta = 2/3$.

Table 5. Experimental Values of the External Mass Transfer-Coefficient and the Surface Diffusivity

β (assumed)	k_{ext} [cm^2/s]	D_s [cm^2/s]	Fisher Test
Tortuosity factor from Eq. 34			
0.66 (E)	0.26	6.34×10^{-7}	1041
0.66 (P)	0.162	4.926×10^{-7}	1281
0.66 (B)	0.103	5.04×10^{-7}	1012
Tortuosity factor from Eq. 35			
0.66 (E)	0.202	3.45×10^{-7}	1197
0.66 (P)	0.139	3.44×10^{-7}	1464
0.66 (B)	0.1	4.23×10^{-7}	1076
1 (E)	0.086	5.57×10^{-7}	1023
1 (P)	0.044	1.44×10^{-6}	1002
1 (B)	0.096	4.59×10^{-7}	498
-1 (E)	0.14	2.45×10^{-7}	3321
-1 (P)	0.136	2.28×10^{-7}	6678
-1 (B)	0.127	2.19×10^{-7}	1×10^4

[a]The symbols E, P, and B denote ethyl, propyl and butylbenzene, respectively.
[b]The values of the external mass-transfer coefficient were calculated for a particle diameter equal to 5.12 μm.

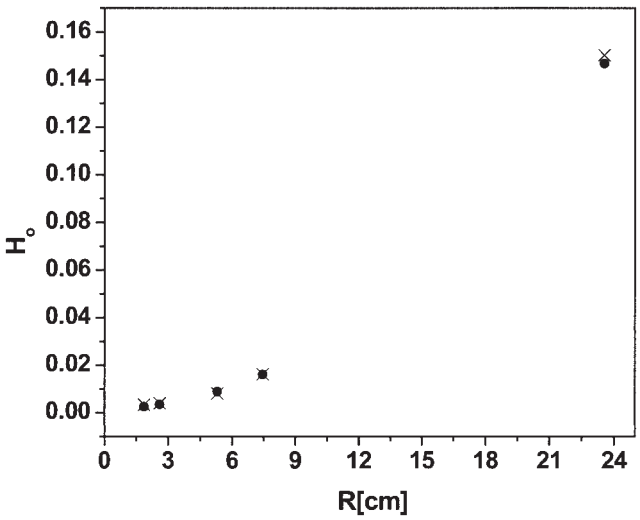

Figure 5. Comparison of exemplary experimental and theoretical value of H_o calculated for propylbenzene and model parameter estimated for $\beta = -1$.

that the rate of the external mass transfer is proportional to the particle diameter. The smallest value of F was obtained for a stagnant fluid phase, F is slightly higher for $\beta = 2/3$ and, surprisingly, the highest of F corresponds to the assumption that $\beta = -1$. A slightly better agreement with the experimental data was achieved when the tortuosity was calculated from Eq. 35. A comparison of the experimental and calculated values of H_o for propylbenzene and for $\beta = -1$ is shown in Figure 5.

Before analyzing further the data in Table 5, the following remark must be made. The differences between the values derived for k_{ext} for different solutes on a given column (hence particle size) may arise only from differences between molecular diffusivities, so the quotient of the external mass-transfer coefficients calculated for the different compounds studied should be proportional to the ratio of their molecular diffusivities. These ratios, calculated from the Wilke-Chang equation, Eq. 24, and the ratios of the experimental external mass-transfer coefficients, are reported in Table 6. It is obvious that the proportionality was observed only for $\beta = -1$ and, moreover, that there is equality between the ratios of the external mass-transfer rate coefficients and of the molecular diffusivities. This suggests that k_{ext} depends linearly on the molecular diffusivity.

Another interesting remark follows from the analysis of the surface diffusivity data in Table 5. Surface diffusivity should decrease with increasing molecular weight of the compound studied in this homologous series. It is obvious that only the data obtained under the assumption that $\beta = -1$ fulfill this requirement. Summarizing: the best and most satisfactory agreement between the current theory of mass transfer in porous media and our experimental results is obtained under the assumption that $k_{ext} = \alpha R$.

This result can be explained by considering the simple Lewis-Whitman stagnant film model.[23] When a fluid flows over a surface, a boundary layer always forms against this surface. The flow velocity in this layer is much lower than in the bulk fluid, so the layer can be regarded as a stagnant film of liquid. From this theory, the following relationship can be derived

$$k_{ext} \approx \frac{D_m}{\delta} \tag{37}$$

where δ is the thickness of the thin film. The main disadvantage of this theory is that it is practically impossible to calculate δ. However, there is a general agreement that this layer thickness decreases with increasing Reynolds number. In the case of our experiments, the Reynolds number increases 13-fold with increasing particle radius. This would explain the important increase of the mass-transfer kinetics, and the increase of k_{ext} with increasing particle size that we have observed.

We understand that the assumption that we have just formulated needs to be verified carefully, under more sophisticated experimental conditions. Such an investigation is now in progress. Nevertheless, in the following, the interpretation of the experimental data is performed assuming the validity of the parameters estimated with the assumption that $\beta = -1$, parameters that are given in Table 5.

Contributions of axial dispersion, external and internal mass-transfer resistances to HETP

The contributions of H_L, H_k, and H_D to the total HETP (see Eq. 14) are plotted in Figure 6, as a function of the particle size, for a mobile phase velocity equal to 1 [ml/min]. The calculations were made for propylbenzene. The largest contribution to the HETP is that of H_D that characterizes the internal mass-transfer resistances. The smallest one is the one due to the external mass-transfer resistances, characterized by H_k. The axial dispersion, characterized by H_L, plays an intermediate role. All these contributions depend on the mobile phase velocity. The dimensionless contributions of these three contributions to the HETP, for mobile velocities of 0.8 and 1.2 [ml/min], are shown in Figures 7 and 8, respectively.

For the smallest particle diameter, at the smallest mobile phase velocity, the contribution of axial dispersion to the HETP prevails over the other two contributions. The relative importance of the internal mass-transfer resistance increases rapidly with increasing particle size and its contribution dominates for particles larger than about 10 [μm]. However, axial dispersion can never be neglected. The contribution of the external mass-transfer resistance is marginal for particle sizes larger than about 15 [μm]. Similar conclusions can be derived from the plots shown in both Figures 7 and 8. It should be noticed,

Table 6. Ratios of the Molecular Diffusivities and the Experimental External Mass-Transfer Coefficients

		k_i/k_i[c]		
i/j[a]	D_{mi}/D_{mj}[b]	$\beta = 2/3$	$\beta = 1$	$\beta = -1$
E/P	1.06	1.45	1.95	1.03
P/B	1.07	1.39	0.46	1.07
E/B	1.13	2.02	0.89	1.1

[a]Symbols E, P and B denote ethyl, propyl and butylbenzene.
[b]Molecular diffusivities from Eq. 24.
[c]Tortuosity parameter from Eq. 35.

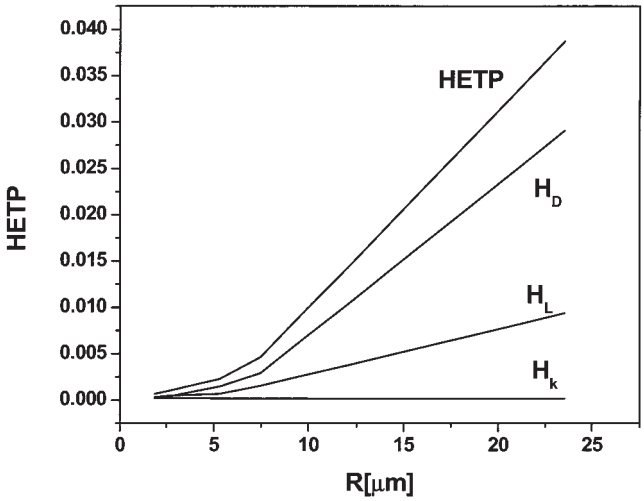

Figure 6. Contributions H_L, H_k, and H_D to the total HETP as a function of the particle radius.

Plot made for propylbenzene.

however, that the importance of the contribution of the internal mass resistance to band broadening increases with increasing mobile phase velocity.

Contributions of pore diffusion and surface diffusion to effective intraparticle diffusion

Equation 33 describes the relationship between the effective diffusivity, D_{eff}, the pore diffusion, D_p, the surface diffusion D_s, and the effective surface diffusion $D_{e,s}$, coefficients. The ratio of these diffusion coefficients is reported in Table 7. The ratio of the surface to the molecular diffusivity is also given. The ratio D_s/D_m is similar to that reported previously.[6] However, the ratio $D_{e,s}/D_p$ is much smaller.[6] This discrepancy comes from the method used to interpret the experimental data. In the previous work, the external mass transfer was calculated from Wilson-Geankoplis correlation Eq. 23 in which the mass-transfer coefficient is inversely proportional to the particle

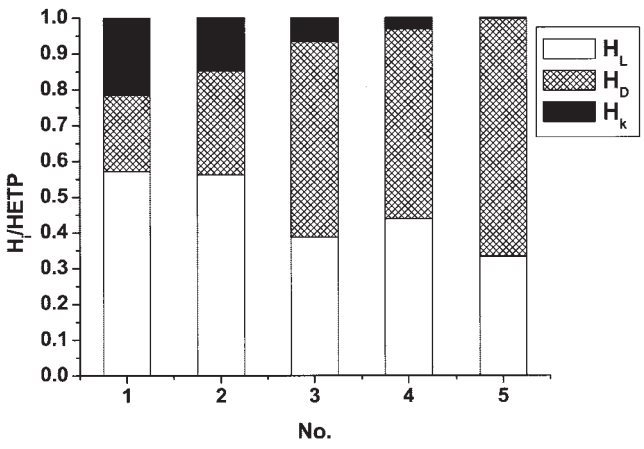

Figure 7. Dimensionless contributions, H_L, H_k and H_D, to the HETP for propylbenzene.

Indexes 1, 2, 3, 4, 5 on the abscissa axis refers to average particle sizes of 3.74, 5.21, 10.6, 14.92 and 47.1 [μm] respectively. Mobile phase velocity, $u = 0.8$ [ml/min].

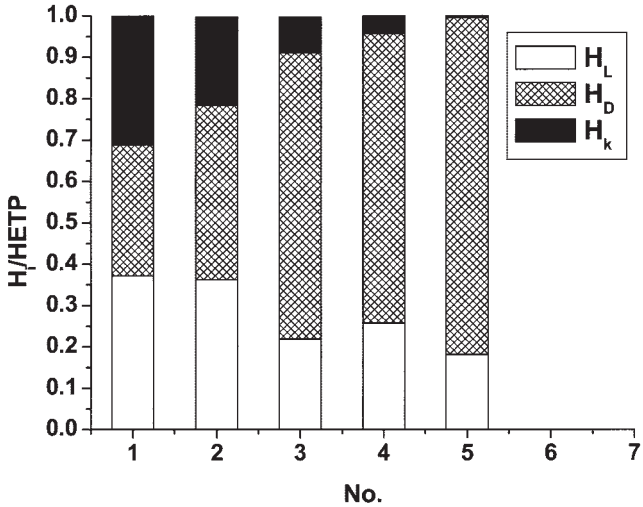

Figure 8. Same as in Figure 7, except mobile-phase velocity, $u = 1.2$ [ml/min].

diameter to the power (2/3). A value of $D_{e,s}/D_p$ similar to the one in Ref. 6, equal to *ca* Eq. 14, could be obtained from the data in this work, if we assume $\beta = 0.66$, and estimate surface diffusivity with the tortuosity factor calculated from Eq. 34.

To avoid possible ambiguities in the interpretation of experimental data, more sophisticated experiments that would allow an independent evaluation of the kinetic rate constants must be undertaken.

Conclusion

Although the apparent dispersion coefficient and the external mass-transfer coefficient may depend on the mobile phase velocity, our experimental results show that this influence is smaller than the experimental errors in the range of velocity investigated. The particle diameter influences the external mass transfer coefficient. The experimental results show that the dependence of the rate constant of the external mass transfer on the particle diameter is not consistent with the Wilson-Geankoplis correlation. This correlation, often used to account for HPLC results, is generally accepted as valid in chemical engineering but it was developed for particle sizes nearly 1,000 times larger than commonly used in contemporary chromatography, and for Reynolds numbers that were, mostly, much larger than those used in liquid chromatography. The range of validity of the correlation is $0.0015 < \mathrm{Re} < 55$ while columns are run usually at $0.001 < \mathrm{Re} < 0.05$, which places them at the very low end of the recommended range of validity of the correlation.

Our experimental results suggest, by contrast, that the exter-

Table 7. Ratios of Effective Surface to Pore Diffusivities and of Surface to Molecular Diffusivities

Solute	$D_{e,s}/D_p$	D_s/D_m
Ethylbenzene	0.67	4.04×10^{-2}
Propylbenzene	1.12	3.97×10^{-2}
Butylbenzene	2.04	4.09×10^{-2}

[a]Symbols E, P, and B denote ethyl, propyl and butylbenzene.
[b]Tortuosity parameter was calculated from Eq. 35.

nal mass-transfer coefficient is proportional to the particle diameter. This result is surprising. The external mass-transfer coefficient does increase linearly with increasing particle size in the investigating range of Reynolds numbers. These results should be considered as preliminary and must be confirmed by carrying out more sophisticated experiments.

Finally, it was also shown that the interpretation of the relative role of pore and surface diffusivity in the internal mass transfer is ambiguous, at least if our results are confirmed. The conclusion on this point will depend on the assumption made on the best model of tortuosity and on the exact relationship between k_{ext}, and the particle size.

Acknowledgment

This work was supported in part by grant CHE-02-44693 of the National Science Foundation, and by the cooperative agreement between the University of Tennessee and the Oak Ridge National Laboratory. We thank Tivadar Farkas (Phenomenex, Torrance, CA) for the generous gift of the columns used in this work and for fruitful and creative discussions.

Notation

A = parameter defined by Eq. 15
C = concentration in the mobile phase
C_p = concentration in the stagnant fluid phase contained inside pores
d = equivalent particle diameter
d_{43} = volume moment mean diameter
D_m = diffusion coefficient
D_{eff} = effective (or inside-pore) diffusion coefficient
D_p = pore diffusivity
D_L = dispersion coefficient
D_s = surface diffusivity
$D_{s,e}$ = effective surface diffusivity
H = high equivalent to theoretical plates
H_L, H_k, H_D = parameters defined by Eq. 14
H_o, H' = parameters defined by Eqs. 16 and 17
k_{ext} = external mass-transfer coefficient
K = equilibrium constant
L = column length
N = number of theoretical plates
M_s = molecular mass
Pe = Peclet number, $uL/D_L\varepsilon_e$
q = concentration of the solute in the stationary phase
r = radial distance from the center of the particle
Re = Reynolds number, $\rho ud/\eta$
R = particle radius
Sc = Schmidt number, $\eta/\rho D_m$
Sh = Sherwood number, $k_{ext}d/D_m$
t = time
T = absolute temperature
u_o = average superficial velocity of the mobile phase
V = volume
V_A = molar volume of solute
x = longitudinal distance along the column

Greek symbols

α_A = association factor
β = exponent of the dependence of the rate constant of external mass transfer on the particle diameter (Eq. 36)
δ = thickness of the thin film
δ_L, δ_f, δ_d, δ_o = parameters defined by Eqs. 7–10
γ = tortuosity parameter
ε_e = external porosity
ε_p = internal porosity
ε_t = total porosity
η = viscosity
μ_1 = absolute moment
μ_2' = second central moment
ρ = fluid density

Subscripts

a = denote adsorbent
i = i-th fraction of adsorbent particle
s = solid phase

Superscript

R = means that parameter depends on used particle radius

Literature Cited

1. Burlington DB, Haggard D, Kaminski E, Sakers F, Grazal J, Whitaker J, King E. A Risk-Based Approach to cGMPs. FDA Report; 2003.
2. Guiochon G, Golshan-Shirazi S, Katti AM. *Fundamentals of Preparative and Nonlinear Chromatography.* Boston: Academic Press; 1994.
3. Ruthven DM. *Principles of Adsorption & Adsorption Processes.* New York; NY: Wiley; (1984).
4. Felinger A, Cavazzini A, Guiochon G. Numerical Determination of the Competitive Isotherm of Enantiomers. *J Chromatogr A* 2003: 986: 207.
5. Bird RB, Stewart WE, Lightfoot EN. *Transport Phenomena,* New York; NY, Wiley, (2002).
6. Miyabe K, Guiochon G. Measurement of the Parameters of the Mass Transfer Kinetics in High Performance Liquid Chromatography. *J Separat Sci* 2003: 26: 155.
7. Wilson EJ, Geankoplis CJ. Liquid Mass Transfer at Very Low Reynolds Numbers in Packed Beds. *Ind Eng Chem Fundam* 1966: 5: 9.
8. Kaczmarski K, Bellot JC. Effect of particle-size distribution and particle porosity changes on mass-transfer kinetics. *Acta Chromatographica* 2003: 13: 22.
9. Kucera E. Contribution to the theory of chromatography. Linear non-equilibrium theory of chromatography. *J Chromatogr* 1965: 19: 237.
10. Kubin M. Collection Czechoslov. *Chem Commun* 1965: 30: 1104.
11. Schneider P, Smith MJ. Adsorption rate constants from chromatography. *AIChE J* 1968: 14: 762.
12. Suzuki M. *Adsorption Engineering.* The Netherlands: Amsterdam; Elsevier, 1990.
13. Miyabe K, Guiochon G. Fundamental interpretation of the peak profiles in linear reversed-phase liquid chromatography. *Adv Chromatogr* 2000: 40: 1.
14. Wilke CR, Chang P. Correlation of diffusion coefficients in dilute solutions. *AIChE J* 1955: 1: 264.
15. Gunn D. Axial and radial dispersion in fixed beds. *Chem Eng Sci* 1987: 42: 363.
16. Chung SF, Wen CY. Longitudinal dispersion of liquids flowing through fixed and fluidized beds. *AIChE J* 1968: 14: 857.
17. Neue UD. *HPLC Columns. Theory, Technology, and Practice.* Wiley–VCH; 1997.
18. Kele M, Guiochon G. Repeatability and reproducibility of retention data and band profiles on reversed-phase liquid chromatography columns—IV. results obtained with luna C18 columns. *J Chromatogr A* 2000: 869: 181.
19. Felinger A, Guiochon G. Validation of a chromatography data analysis software. *J Chromatogr A* 2001: 913: 221.
20. Halasz I, Martin K. Pore Sizes of Solids. *Angew Chem.* (Int. Ed. Engl.) 1978: 17: 901.
21. Guan H, Guiochon G. Study of the physico-chemical properties of some packing materials. I. measurement of the external porosity of packed columns by inverse size exclusion chromatography. *J Chromatogr A* 1996: 731: 27.
22. Fletcher R. *A modified Marquardt subroutine for nonlinear least squares.* AERE-R6799—Harwell.
23. Skelland AHP. *Diffusional Mass Transfer.* New York: Wiley; 1974.

Manuscript received Dec. 20, 2004, and revision received Apr. 7, 2005.